INDIAN JOURNAL OF SCIENCE AND TECHNOLOGY

RESEARCH ARTICLE

Modeling Extreme Values of Non-Stationary Precipitation Data with Effects of Covariates

K M Sakthivel[1]*, V Nandhini[2]

1 Professor, Department of Statistics, Bharathiar University, Coimbatore-46, Tamil Nadu, India
2 Research Scholar, Department of Statistics, Bharathiar University, Coimbatore-46, Tamil Nadu, India

OPEN ACCESS

Received: 07-03-2024
Accepted: 07-05-2024
Published: 29-05-2024

Citation: Sakthivel KM, Nandhini V (2024) Modeling Extreme Values of Non-Stationary Precipitation Data with Effects of Covariates. Indian Journal of Science and Technology 17(22): 2283-2295. https://doi.org/10.17485/IJST/v17i22.655

* **Corresponding author**.

sakthithebest@buc.edu.in

Funding: None

Competing Interests: None

Published By Indian Society for Education and Environment (iSee)

ISSN
Print: 0974-6846
Electronic: 0974-5645

Abstract

Background/Objectives: Climate change is one of the most challenging problems of recent decades as it is highly volatile and needs a very effective scientific approach to find a solution. Further, the changes in the climate especially extreme cases have a more negative influence on day to day affairs of society. Hence, developed countries pay much attention to climate change and make policies at a global level. To find the scientific solution for these kinds of climate change, Extreme value theory offers effective methods for estimating and quantifying these types of natural hazards associated with climate. **Methods:** Block (Annual) maxima and peak over threshold are two strategies employed in this theory. The data observed on precipitation are mostly having non-stationary characteristics along with covariates. The generalized extreme value distribution and generalized Pareto distribution are used to model this type of non-stationary stochastic process. **Findings:** This study proposes a pragmatic automated dual-phase threshold selection technique that employs the entropy method to combine the results from various goodness of fit tests into a single unified measure known as the evaluation indicator, resulting in an efficient threshold for capturing extreme values. This allows for a more comprehensive examination of various thresholds using evaluation indicators and avoids assessing each test criterion individually. **Novelty:** In contrast to the subjective results of threshold stability plots, the dual-phase technique is based on numerical computations, which reduce bias and improve decision-making objectivity. We illustrate the applicability of the proposed technique by analyzing a precipitation dataset that includes time and wind speed as covariates. The results of the comparative analysis reveal that the proposed automated dual-phase threshold approach outperforms the peaks over threshold and annual maxima methods.

Keywords: Non-stationary; Extreme values; Annual maxima; Threshold selection; Evaluation indicator

1 Introduction

In recent years, the changes in weather and climate have serious implications for the world economy. For example, drought may negatively impact both food production and human health, and floods can spread illness, damage infrastructures, and devastate ecosystems. A shift in temperature change will lead to adverse effects in certain geographical regions around the globe. Therefore, the impact of climate change is considered the biggest challenge in the 21st century both at regional and international levels. In particular, the extreme events of precipitation have serious effects, including a considerable decline in agricultural production, an increase in energy demand and generation, a supply of water resources, uncontrolled price variation in essential commodities, and the loss of human life. The primary issue encountered here is how to model these types of data and forecast such extreme events well in advance. Extreme value analysis is a major statistical approach for evaluating, comprehending, and forecasting natural hazard occurrences such as drought and flood. To reduce the likelihood of having a major disaster, extreme value theory (EVT) was utilized to design a reliable framework under a wide range of circumstances. The estimation of rainfall during various return periods is essential for the planning and construction of drainage systems, bridge and dam maintenance, and flood risk assessment. The usual assumption in such analyses is that the parameters representing the probability distribution are stationary and hence do not vary with time. Applying these principles in stationary settings can provide invaluable insights for planning, decision-making, and estimating the impact of unwanted events and weather patterns. It is crucial to have concepts that can be used to examine the non-stationary nature of hydrological and climactic extremes. Numerous studies were available in the literature to investigate the potential consequences of climate change using the non-stationary models, and they are: Ouarda and Charron (2019) [1] presented that non-stationary frequency analysis that combines trends and climate variability by including covariates in the distribution parameters. Kumar et al. (2021) [2] investigated the extreme climatic elements such as extreme air temperature, low relative humidity, and severe winds as covariates, for daily, monthly, and annual rainfall values reported at the Narora site. Baldan et al. (2022) [3] investigated the importance of non-stationary with linear dependence in parameters of generalized extreme value (GEV) distribution and point process model for assessing extreme sea levels. Rohmer et al. (2021) [4] discussed that non-stationarity in heavy rainfall time series is often apparent in the form of trends because of long-term climate changes. Prahadchai et al. (2022) [5] built sixteen non-stationary models for time-dependent functions of the location and scale parameters of the GEV to the annual maximum (AM) daily and 2-day precipitation data observed from Thailand. Kim et al. (2022) [6] present a new method for modeling extreme rainfall values in South Korea, this procedure identifies significant seasonal climate indices (SCIs) that influence the long-term trend of AM daily rainfall using statistical techniques such as ensemble empirical mode decomposition and then selects an appropriate GEV distribution among stationary and nonstationary GEVs using time and SCIs as covariates. Wang et al. (2022) [7] developed a new non-stationary standardized runoff index by combining climate indices and modified reservoir index as explanatory variables using the generalized additive model for location, scale, and shape for the hydrological drought inspection of the Hanjiang River basin in China. Kumar et al. (2023) [8] investigated the risk of extreme precipitation/discharge indicators using non-stationary GEV models with covariates, then the machine learning models and a conceptual water balance model were calibrated on a monthly measure for discharge estimation. Khan et al. (2023) [9] intended to analyze the effects of nonstationarity in precipitation of Southern Punjab, Pakistan on employing the four frequency distributions: GEV, Gumbel, normal, and lognormal. The results of the non-stationarity revealed a variety of impacts across regions, including an increase or decrease in the return amount of intense precipitation.

The threshold techniques for climatic variables are widely used to estimate extreme quantiles and distribution tails. Peaks over threshold (POT) techniques have the advantage of being able to consider significantly more data than the AM method since they take into account every datum over the threshold rather than selecting only one value (highest or lowest) for each block or year. The difficulty is that if a high threshold is used, only a few data points increase the variation of the estimates. However, if the threshold is set too low, a bias can arise. To overcome such difficulties, several procedures came into existence, we mentioned few recent research that is: Wu and Qiu (2018) [10] propose a multiple criteria decision analysis (MCDA) approach using the different test statistic values of goodness of fit test criterion for selecting a threshold in the peak over threshold method, providing insights into its potential for improving extreme value estimation in vehicle load analysis. Galib et al. (2022) [11] developed the DeepExtrema a novel framework that forecasts a time series' block maximum value through the combination of a deep neural network along with GEV distribution. Pahrany et al. (2024) [12] devised an automated threshold selection approach that uses the distribution of the difference in parameter estimations when the threshold is adjusted and applies it to published claim severity.

In this paper, we proposed an entropy-based automated dual-phase threshold (DPT) method that is useful to make decisions on threshold selection based on the normalization of goodness of fit test results. We provide a novel analytical DPT technique for filtering extreme events to track climate change and demonstrate its distinct consequences on certain regions. The primary goals of this research are to (a) determine an optimal threshold using the proposed automated DPT and compare its performance to the classical POT and AM methods, and (b) identify the most appropriate distribution function in the context of stationary

and non-stationary assumptions of extreme precipitation. This study provides a more comprehensive analysis of observed changes in precipitation extremes in seven major districts of Tamil Nadu state, India, during the period 1991-2023, by applying stationary and non-stationary EVT tools. In a non-stationary framework, the interpretation of extreme precipitation for specific return periods becomes challenging due to a time-dependent exceedance probability. In this study, return-level estimates of extreme events in non-stationary situations are calculated using the end of the data period (i.e.,) the year 2023. The results of this study highlight the significance of the selected covariate and its integration in the development of the model. The paper is structured as follows: Section 2 presents the classical and proposed methodologies of extreme value theory; Section 3 provides stationary and non-stationary models. Section 4 discusses the preliminary data analysis and its results, followed by a summary and conclusion in Section 5.

2 Methodology

In extreme value analysis, the block maxima or annual maxima and peaks over the threshold are the two classical approaches (Coles, 2001) [13]. This section depicts the distinctive features of conventional and proposed extreme-value techniques, resulting in substantial improvements in this theory.

2.1 Annual Maxima

The annual maxima approach discovers extreme values by taking the maximum values from observational data that have been structured into a specific block or period. The Fisher-Tippett theorem states the rescaled sample maxima converge in distribution to a variable having a generalized extreme value distribution

Theorem 1: (Fisher Tippett Theorem, 1928)Let $X_1, X_2, \ldots, X_n$ be an independent and identically distributed random sequence with distribution function F. The normalizing sequences $a_n > 0$, $b_n \in R$ such that $\frac{M_n - b_n}{a_n}$ converges in distribution, so that

$$\lim_{n\to\infty} P\left(\frac{max\,(X_1, X_2, \ldots, X_n\} - b_n}{a_n} \leq x\right) = \lim_{n\to\infty} F^n\,(a_n x + b_n) \to G\,(x) \tag{1}$$

where G can be described as a non-degenerate distribution function. The convergence in (Equation (1)) occurs if and only if $n\{1 - F^n\,(a_n x + b_n)\} = -logG\,(x)$. It is understood that G must belong to one of the three categories of limiting distributions, including Gumbel, Fréchet, and Weibull. These three categories can be combined to form a single generalized extreme value distribution. The cumulative distribution function of the three-parameter generalized extreme value distribution with location parameter μ, shape parameter ξ, scale parameter σ is given by

$$G\,(x) = exp\left\{-\left(1 + \xi\left(\frac{x-\mu}{\sigma}\right)\right)^{-1/\xi}\right\} \tag{2}$$

Define, for $\left\{x : 1 + \xi\left(\frac{x-\mu}{\sigma}\right) > 0\right\}$, $\mu \in R$, $\sigma > 0$ and $\xi \in R$ may be any real numbers, the case $\xi = 0$ being interpreted as the limit $\xi \to 0$,

$$G\,(x) = exp\left\{-exp\left(-\left(\frac{x-\mu}{\sigma}\right)\right)\right\} \tag{3}$$

which is widely called the Gumbel distribution. The shape parameter ξ (extreme value index) can decide the tail behavior of the distribution. The case $\xi > 0$ is that of the polynomially decreasing tail function and therefore corresponds to a long-tailed parent distribution (Fréchet). The case $\xi < 0$ is the case of a finite upper endpoint and therefore short-tailed (Weibull) respectively.

2.2 Peaks over Threshold

The peaks-over-threshold approach is also called the method of excess. The POT approach evaluates the distribution of exceedances above the specified threshold. Furthermore, it can be shown that for some sufficiently large threshold u, the distribution of the values exceeding the threshold is approximated to a GP distribution.

Theorem 2: (Pickands-Balkema-De Haan theorem, 1975) Let $X_1, X_2, \ldots, X_n$ be a sequence of iid random variables, and let F_u be their conditional excess distribution function. This theorem posed that for a large class of underlying distribution F, and

large u, F_u is well approximated by the GP distribution. That is: $F_u(x) \approx G_{\xi,\sigma}(x)$ as $u \to \infty$. The cumulative distribution function of the GP distribution with shape parameter ξ and scale parameter σ has the following representation

$$G_{\xi,\sigma}(y) = \begin{cases} 1-\left(1+\xi\left(\frac{x}{\sigma}\right)\right)^{-1/\xi}; & if\ \xi \neq 0 \\ 1-e^{-\left(\frac{x}{\sigma}\right)}; & if\ \xi = 0 \end{cases} \quad (4)$$

where, i) $x \geq 0$ when $\xi \geq 0$ and $0 \leq x \leq -\sigma/\xi$ when $\xi < 0$ and ii) $\sigma > 0$ when $\xi = 0$. When $\xi > 0$ obtaining the ordinary Pareto distribution. When $\xi = 0$ obtains the exponential distribution. When $\xi < 0$ obtaining the short-tailed Pareto distribution. The main difficulty of modeling with the POT method is setting the right threshold. It is important to find a good balance in setting the threshold to obtain a suitable balance between variance and bias of the model. The parameter stability plot also called the threshold stability plot is one of the threshold selection methods by visualization (Coles, 2001; Scarrott and MacDonald, 2012)[13,14]. This method is to study the stability of the parameter in the plots which are also based on the threshold stability property of the GP distribution. The parameter stability plot shows how the shape and modified scale parameters of the GP change over a range of threshold values. The idea is that these parameters should be stable within a range of valid thresholds.

2.3 Dual-Phase Threshold Selection-A Proposed Approach

In this section, an appropriate threshold can be obtained by multiple testing procedures after trimming non-extremes from the series which can be described using the following formalized dual-phase threshold selection algorithm:

Phase 1: Trimming of non-extremes: Let $X_1, X_2, \ldots, X_n$ be an independent and identically distributed random sample of size n. The procedure is discussed as follows:

- **Step 1:** The sequential testing of the statistical hypothesis can be used to choose the most suitable threshold. The null hypothesis can be stated as: $H_0^{(i)}$: The distribution of the exceedances n_i above the chosen threshold follows the GP distribution.
- **Step 2:** The sequence of the null hypothesis $H_0^{(1)}, H_0^{(2)}, \ldots, H_0^{(k)}$ can be evaluated using goodness of fit tests that are available in the literature. For illustration, the two commonly used goodness of fit tests which are the Kolmogorov-Smirnov (K-S) test and Cramer von Mises (CvM) test with $\alpha = 0.05$ a level of significance has been performed in this case. The test statistic values are denoted as ω_{ij} and its p-values are $p_{ij} \in [0,1]$ for $i \in 1,2,\ldots,k$, $j \in 1,2,\ldots,l$ denotes the k hypothesis and l test criteria.

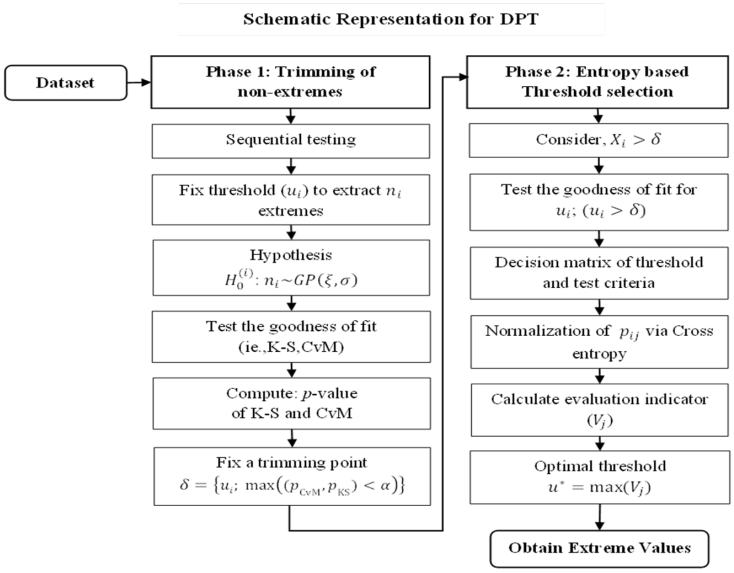

Fig 1. Flowchart for DPT method

- **Step 3:** If the p-value $p_{ij} > \alpha$, then the null hypothesis $H_0^{(i)}$ can be accepted. Otherwise, the null hypothesis is to be rejected for any $p_{ij} < \alpha$ can be represented as $H_0^{(r)}; r \in 1,2,\ldots,k-1$ correspond to the chosen threshold.
- **Step 4:** If $H_0^{(r)}$ is rejected, then the threshold u_r can be terminated from the sequence of thresholds, the values below u_r are considered to be non-extremes, and then the refined sequence of thresholds be $u_{r+1} < u_{r+2} < \cdots < u_k$, can be considered for the study. The process of testing can be repeated until all the null hypotheses for the refined range of thresholds are accepted to show that the exceedances above the thresholds follow the GP distribution.
- **Step 5:** To remove the non-extremes, in some cases, both the KS and CvM test spots, $p_{ij} < \alpha$ at different associated thresholds, on such occasions, we choose the trimming point as $\delta = \{u_i; max((p_{CvM}, p_{KS}) < \alpha)\}$ respectively.
- **Step 6:** The trimming point δ can be fixed, the values over this point $X_i > \delta$ are considered as the subsample observation. Here, the values $X_i < \delta$ can be terminated from the series. The values above δ can be considered for choosing an appropriate threshold through the following procedure.

Phase 2: Entropy-based Threshold Selection: Let us consider a set of threshold values, the trimming point δ followed from phase 1, which can be considered as the initial value for the range of threshold until the 99$^{\text{th}}$ percentile with 0.01 varying levels. There exists an nk exceedances, $k = 1,2,\ldots,m$ for each threshold. In this phase, we choose the optimum threshold by evaluating the p-values using the entropy method that can be applied to determine the weights of the p-values of the goodness of fit test criteria of GP distribution. The p-value of a test will be determined for each threshold using multiple criteria. Entropy-based weighting can be used to improve the precision of goodness of fit tests in threshold choice. It prioritizes tail data and improves model fit assessment in significant extreme values, which leads to more reliable extreme value analysis.

- **Step 1:** The decision matrix can be established by the test criteria p-values that are achieved by evaluating the range of threshold exceedances. The number of evaluating thresholds A_i are m and the test criteria are n, d_{ij} representing the performance value of the i^{th} threshold to the j^{th} criteria for the decision matrix D, (i.e.,) $D = (d_{ij})_{m\times n}$ such as follows

$$D = \begin{array}{c} \\ A_1 \\ A_2 \\ \vdots \\ A_m \end{array} \begin{array}{c} \begin{array}{cccc} C_1 & C_2 & \ldots & C_l \end{array} \\ \begin{bmatrix} d_{11} & d_{12} & \ldots & d_{1l} \\ d_{21} & d_{22} & \ldots & d_{2l} \\ \vdots & \vdots & & \vdots \\ d_{m1} & d_{m2} & \ldots & d_{ml} \end{bmatrix} \end{array} \tag{5}$$

Where the vector A_j represents the threshold and the vector C_j represents the criteria for $i = 1,2,\ldots,l$ and $j = 1,2,\ldots,m$ respectively.

- **Step 2:** In multiple tests, the p-values can be smoothed to control the overall fluctuation rate of different test criteria. The normalized values for different chosen criteria (Zhu et al., 2020; Duc Trung, 2021) [15,16] can be determined as

$$p_{ij} = \frac{d_{ij}}{m + \sum_{i=1}^{m} (d_{ij})^2} \tag{6}$$

where d_{ij} is the value of the j^{th} criterion corresponding to the i^{th} threshold, and m is the number of taken threshold values. Then the normalization decision matrix is defined as $p = (p_{ij})_{m\times n}$.

- **Step 3:** The entropy measurement values for each criterion can be calculated. The cross-entropy can be defined as

$$E_j = -\sum_{i=1}^{m} (p_{ij} log\,(p_{ij})) - \left(1 - \sum_{i=1}^{l} p_{ij}\right) \left(log\left[1 - \sum_{i=1}^{l} p_{ij}\right]\right) \tag{7}$$

- **Step 4:** The relative significance of each criterion can be computed using

$$w_j = \frac{1 - E_j}{\sum_{j=1}^{m} (1 - E_j)} \tag{8}$$

This is the reasonable expression of normalized weighted value, $\sum_{j=1}^{m} w_j = 1$, for $w_j \in [0, 1]$.

- **Step 5:** The evaluation indicator (V) can be calculated as

$$V_j = \sum_{j=1}^{n} w_j d_{ij} \tag{9}$$

where, w_j is the weight of each criterion d_{ij}. The evaluation indicator values can be ranked based on the principle of choosing the best threshold by having the maximum of V_j, that is $u^* = max(V_j)$. The maximum value of the evaluation indicator V_j of the p-values of multiple goodness of fit test criteria corresponds to the range of chosen threshold exceedances which indicates a better fit of the GP distribution. The threshold u^* is considered to be optimum, and the exceedances above this point are taken as extreme values that can be modeled with the generalized Pareto distribution. The DPT method tests the multiple thresholds to find the best fit for the extreme value model and adjusts p-values to control the error rate and select the most appropriate threshold.

2.4 Stationary and Non-stationary Models

In the context of non-stationarity, we might have time-varying parameters. This could be due to trends, seasonality, or other factors influencing extreme events. In the non-stationary case, the parameters are expressed as a function of covariates such as time: $GEV(\mu_t,\ \sigma_t, \xi_t)$ and $GP(\sigma_t, \xi_t)$ models.

Table 1. The stationary and non-stationary models with varying parameters

Models	Parameter forms	Remarks
Stationary and Non-stationary GEV Models		
GEV00	μ (constant), σ (constant), ξ (constant)	Stationary Model
GEV10	$\mu_t = \mu_0 + \mu_1 Y_t$, σ (constant), ξ(constant)	A non-stationary model with linear dependence of the location parameter on covariate Y_t
GEV01	$log\sigma_t = \sigma_0 + \sigma_1 Y_t$,$\mu$ (constant), ξ (constant)	A non-stationary model with linear dependence of the scale parameter on covariate Y_t
GEV11	$\mu_t = \mu_0 + \mu_1 Y_t$, $log\sigma_t = \sigma_0 + \sigma_1 Y_t$, ξ (constant)	A non-stationary model with location and scale parameters linearly depends on a covariate Y_t
GEV20	$\mu_t = \mu_0 + \mu_1 Y_t + \mu_2 {Y_t}^2$, σ (constant), ξ(constant)	A non-stationary model with a location parameter is a quadratic function of a covariate Y_t
GEV02	$log\sigma_t = \sigma_0 + \sigma_1 Y_t + \sigma_2 {Y_t}^2 \mu$ (constant), ξ(constant)	A non-stationary model with a scale parameter is a quadratic function of a covariate Y_t
GEV12	$\mu_t = \mu_0 + \mu_1 Y_t$, $log\sigma_t = \sigma_0 + \sigma_1 Y_t + \sigma_2 {Y_t}^2$, ξ(constant)	A non-stationary model with location is linear and the scale parameter is a quadratic function of a covariate Y_t
GEV21	$\mu_t = \mu_0 + \mu_1 Y_t + \mu_2 {Y_t}^2$, $log\sigma_t = \sigma_0 + \sigma_1 Y_t$,$\xi$(constant)	A non-stationary model with location is quadratic and the scale parameter is a linear function of a covariate Y_t
GEV22	$\mu_t = \mu_0 + \mu_1 Y_t + \mu_2 {Y_t}^2$, $log\sigma_t = \left(\sigma_0 + \sigma_1 Y_t + \sigma_2 {Y_t}^2\right)$, ξ(constant)	A non-stationary model with location and scale parameters is a quadratic function of covariate Y_t
Stationary and Non-stationary GP Models		
GP	σ(constant), ξ(constant)	Stationary Model
NSGP1	$log\sigma_t = (\sigma_0 + \sigma_1 Y_t)$, ξ(constant)	A non-stationary model with scale parameters is a linear function of covariate Y_t

Continued on next page

Table 1 continued

NSGP2	$log\sigma_t = \left(\sigma_0 + \sigma_1 Y_t + \sigma_2 {Y_t}^2\right)$, ξ(constant)	A non-stationary model with scale parameters is a quadratic function of covariate Y_t
NSGP3	$log\sigma_t = \left(\sigma_0 + \sigma_1 sin\left(\frac{2\pi Y_t}{365}\right)\right)$, ξ(constant)	A non-stationary model with scale parameter is a sinusoidal function of time-dependent covariate Y_t
NSGP4	$log\sigma_t = \left(\sigma_0 + \sigma_1 sin\left(\frac{2\pi Y_t}{365}\right) + \sigma_2 cos\left(\frac{2\pi Y_t}{365}\right)\right)$, ξ(constant)	A non-stationary model with scale parameter is a sinusoidal function of time-dependent covariate Y_t

Let $\phi_t = log\,(\sigma_t)$ be the transformation used to ensure the positive values of scale parameters while estimating the parameters. The trend and dependence on covariates are often characterized by a change in the location and the scale parameters. For the non-stationary GEV and GP models, it is difficult and important to estimate the shape parameter precisely. Therefore, this study assumes the shape parameter to be constant over time. A conditional GP distribution with time-varying parameters can approximate the tail beyond a given threshold. The maximum likelihood estimation approach can be used to estimate the parameters and information criteria measures are utilized to select the best model.

3 Results and Discussion

The daily maximum precipitation (mm/day) data observed over the flood-affected regions of Tamil Nadu along with wind speed (m/s) as a covariate has been considered in this study. The precipitation and wind speed data can be taken from the website of NASA's Goddard Earth Sciences Data and Information Services Center (GES DISC). The GES DISC is the primary distribution center for MERRA-2 data. MERRA-2, or the Modern-Era Retrospective Analysis for Research and Applications, is a reanalysis dataset produced by NASA's Global Modeling and Assimilation Office (GMAO). We have selected the seven flood-affected regions (R) of Tamil Nadu, India; its latitude and longitude with maximum precipitation level for region R1 is Chennai (13.0827°N, 80.2707 °E) with 178.98 mm/day, region R2 is Chengalpattu (12.6819°N, 79.9888 °E) with 156.79 mm/day, region R3 is Thoothukudi (8.7642 °N, 78.1348 °E) with 183.82 mm/day, region R4 is Tirunelveli (8.7131 °N, 77.7567 °E) with 229.03 mm/day, region R5 is Ramanathapuram (9.4071 °N, 78.7023 °E), with 108.27 mm/day, region R6 is Virudhunagar (9.568 °N, 77.9624 °E)) with 151.12 mm/day and region R7 is Kanniyakumari (8.0883°N, 77.5385 °E) has 225.26 mm/day respectively. The Mann Kendall (MK) and KPSS tests were first used to determine whether the daily maximum precipitation dataset met the assumptions of stationarity and trend. The MK test shows the degree of correlation between the time and daily maximum series by computing the τ value, the positive value indicates an increasing trend, and the negative value indicates a decreasing trend. Since the p-value was smaller than the 5% level of significance in the regions, the null hypothesis (H_0) that there is no monotonic trend in the series was rejected and the alternative hypothesis (H_1) that there is a monotonic trend in the series can be confirmed. In addition, it can be seen that region R3 has a significant trend which is shown in Table 2.

Table 2. The trend and stationary test results

Region		R1	R2	R3	R4	R5	R6	R7
MK	τ	0.0415	0.0615	0.0086	0.0519	0.0163	0.0258	0.0793
	***p*-value**	<0.05	<0.05	0.1645	<0.05	<0.05	<0.05	<0.05
KPSS	**Level**	0.1199	0.2054	2.0164	1.6088	0.3977	1.2955	1.1924
	***p*-value**	0.1	0.1	0.01	0.01	0.08	0.01	0.01

Then, the KPSS tests were used to test the null hypothesis H_0 as stationary in the series of maximum precipitation over the study area shown in Table 2. The H_0 can be accepted if the p-value is greater than the 5% level of significance. Thus, the regions R1, R2, and R5 show stationarity and the remaining regions show a non-stationary nature in the series. However, trend tests are not always effective in detecting nonstationarity. On the other hand, this issue will be studied in more detail, where the location and scale parameters of the GEV distribution and the scale parameters of the GP distribution have been modified depending on the covariate, and the influence of non-stationary was determined on the model performance.

In this application of the non-stationary models, the main objective is to study the conditional distribution of the daily maximum precipitation (X) as a function of the wind speed (m/s). For non-stationary models, the inclusion of covariates improves the description of the process that generates data but also increases the number of parameters that must be considered. This section describes the extensive application of both non-stationary and stationary models in all seven locations to estimate extreme precipitation employing the best model for each region. The present study attempted to examine the characteristics of

Table 3. The GEV models selection for the AM series in region R1

Param	GEV00	GEV10	GEV01	GEV11	GEV20	GEV02	GEV12	GEV21	GEV22
ξ	0.1793 (0.1475)	0.0547 (0.1563)	-0.1370 (0.1445)	-0.0151 (0.1358)	0.0253 (0.1263)	0.0451 (0.1580)	-0.0165 (0.1376)	-0.0143 (0.1362)	-0.0120 (0.1427)
μ	65.3672 (4.0517)	-	60.3037 (4.3163)	-	-	65.9615 (3.9205)	-	-	-
σ	20.3985 (3.1823)	19.1065 (2.9443)	-	-	19.0048 (2.7056)	-	-	-	-
μ_0	-	31.9055 (14.6738)	-	25.5457 (8.9184)	63.1338 (27.2187)	-	24.6866 (9.0908)	31.2119 (23.5555)	33.6187 (18.6042)
μ_1	-	5.7609 (2.4205)	-	6.8603 (1.6675)	-5.2621 (8.6869)	-	7.0430 (1.7597)	4.7044 (8.5899)	3.2842 (7.1629)
μ_2	-	-	-	-	0.8821 (0.6569)	-	-	0.1857 (0.7344)	0.3512 (0.6369)
σ_0	-	-	1.9522 (0.4369)	1.6287 (0.4515)	-	5.3072 (1.7369)	1.1987 (1.6179)	1.6445 (0.4681)	0.7049 (1.8167)
σ_1	-	-	0.1844 (0.0737)	0.1904 (0.0665)	-	-0.8476 (0.5182)	0.3297 (0.5081)	0.1878 (0.0688)	0.4943 (0.5758)
σ_2	-	-	-	-	-	0.0683 (0.0355)	-0.0102 (0.1376)	-	-0.0227 (0.0422)
AIC	316.076	308.868	314.739	302.698	309.332	312.446	304.622	304.648	306.392
BIC	320.565	314.854	320.726	310.181	316.814	319.928	313.601	313.627	316.868
AICc	316.903	310.296	316.166	304.920	311.554	314.668	307.853	307.878	310.872
HQIC	317.586	310.882	316.752	305.215	311.849	314.963	307.643	307.669	309.916

precipitation extremes in Tamil Nadu. Specifically, two regions: Chennai and Thoothukudi were chosen among the seven, based on population for illustrative purposes. All cities have the longest record of 33 years (1991-2023). Here, we demonstrated the fit of the GEV model for AM and the GP model for the POT, and DPT series. The extreme rainfall in each year is identified as the observations of the annual maxima series. The GEV fits with maximum likelihood estimation to annual maximum extremes of all the seven regions. In this case, we compared eight non-stationary GEV models with one stationary model. The information criteria results in Table 3 were utilized to compare the performance of the models in stationary and non-stationary instances to investigate model supremacy. The stationary GEV00 model is appropriate for the yearly maximum series for regions R3, R4, and R5. The non-stationary GEV10 model performs best for regions R2 and R6, followed by GEV11 for R1 and GEV22 for R7 respectively. Table 5 shows the results of the non-stationary and stationary models in each region for daily maximum precipitation data. This table describes that, the three regions with stationary GEV models and the four regions that benefit from the non-stationary GEV models among these seven regions for the annual maximum series. Precipitation extremes from annual maxima account for only one maximum value for every year, but the threshold-based method accounts for many extreme events within a single year. The threshold is determined using the two different approaches, POT and DPT, for the daily maximum precipitation values. When using the POT method, the suitable threshold must be chosen carefully with GP parameter estimates. The parameter stability plots are graphical tools for determining the threshold, which involves plotting the modified scale parameter and the shape parameter against the prefixed threshold range of 80-99th percentile. A threshold u from POT can be obtained from the parameter stability plot for regions R1 and R2 which has been displayed in Figure 2 **(a)** represents the modified scale parameter plot and **(b)** represents the shape parameter plot. The dark black middle line in the figures represents the estimated values, the bounded dotted line denotes its confidence interval and the vertical line represents the threshold marked at the location where the parameter estimates show suitable stability. The parameter estimates should be stable above the threshold at which the GP model becomes valid. In some cases, identifying accurate stability in parameter estimates is difficult in the classical parameter stability plot and it is not suitable for finding an optimum threshold. In such cases, the proposed DPT method serves as an alternative to the choice of threshold.

The threshold u^* can be obtained from the DPT method by implementing the cross entropy to evaluate and generate relative weights to the goodness of fit test criteria values. There are several tests available in the literature, here we choose two primary tests as Kolmogorov-Smirnov (KS) test and the Cramer von Mises (CvM) test. It can be used for decision-making in the context of threshold selection and measure how well the distribution fits the extreme values that are extracted from the entire daily

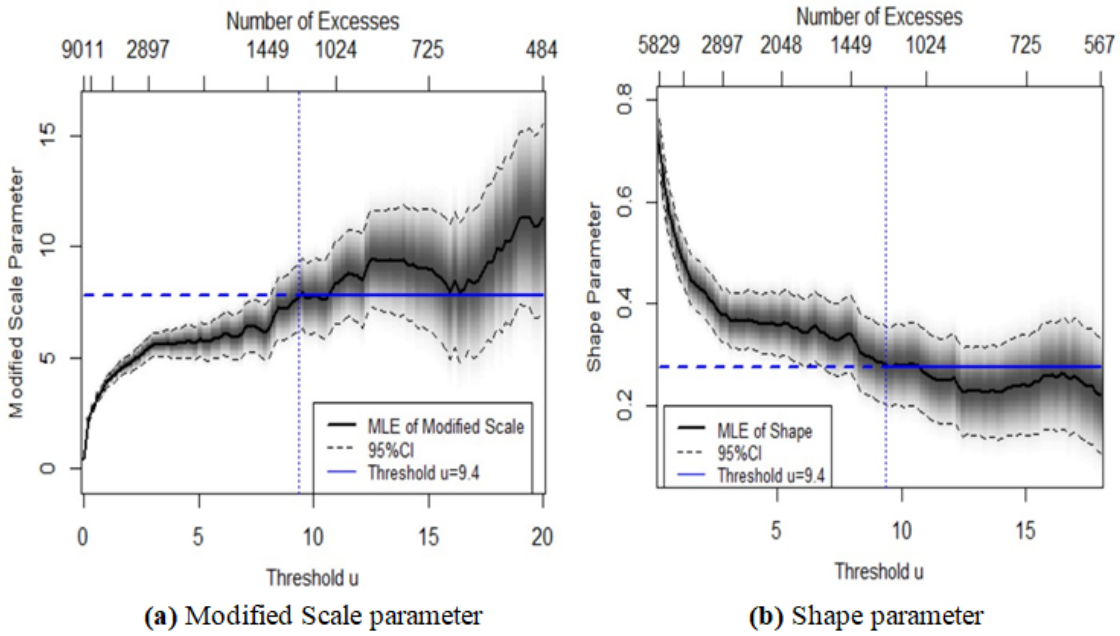

(a) Modified Scale parameter **(b)** Shape parameter

Fig 2. Parameter Stability Plot for region R1

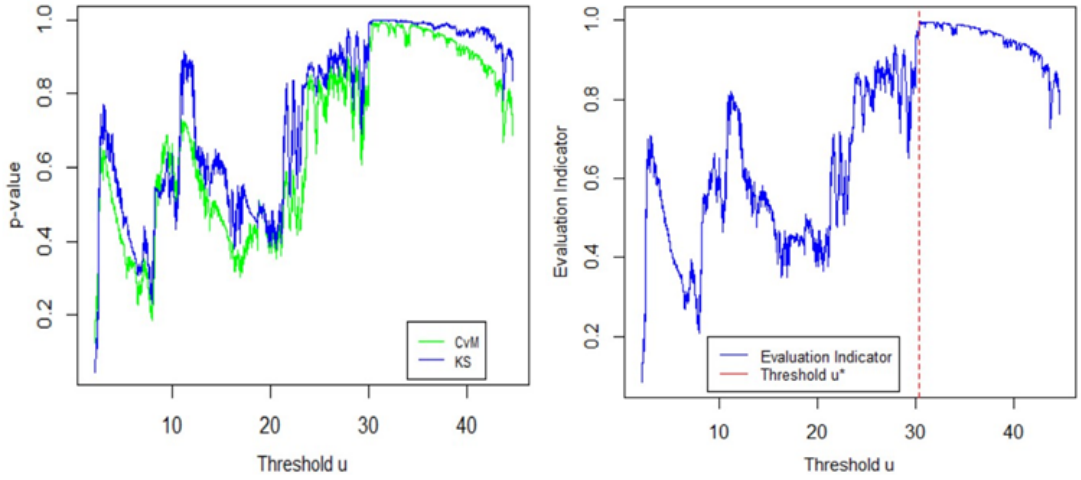

(a) The goodness of fit *p*-value plot **(b)** Evaluation indicator plot

Fig 3. The p -value plot and evaluation indicator plot for R1

maximum precipitation series. Figure 3 **(a)** has their *x*-axis representing the threshold value and *y*-axis representing the *p*-values, indicating the probability values of two different criteria associated with the chosen thresholds. The goodness of fit *p*-value plots provides significant visual insights regarding the degree of agreement between the data and theoretical distribution. Making a decision requires an understanding of the plot and the interpretation of *p*-values under the chosen criterion. The different goodness of fit test criteria result in modest changes in obtaining the highest possible values; it does not always lie at the same spot, and raw *p*-values might be misleading. The entropy weights can be used to aggregate *p*-values from goodness-of-fit tests, indicating the relative measures of each test. The values of an evaluation indicator shown in Figure 3 **(b)** provide insights into choosing the best threshold. The evaluation indicator in this figure exhibiting the greatest value suggests that the chosen threshold is reasonable. The threshold values obtained for region R1 from the POT is u=9.4 has its subsample size (n)=1203, and the DPT has u^*=30.4 and its n=241 for R1. The POT extremes in R1 can also be evaluated for the GPD fit with maximum

likelihood estimates.

Table 4. The estimated values of parameters from POT and DPT with the GP model for region R1

Param	Peaks over Threshold					Dual-Phase Threshold				
	GP	NSGP1	NSGP2	NSGP3	NSGP4	GP	NSGP1	NSGP2	NSGP3	NSGP4
ξ	0.2755 (0.0391)	0.0286 (0.0318)	0.0284 (0.0318)	0.2752 (0.0390)	0.2759 (0.0391)	0.0397 (0.0668)	-0.1642 (0.0575)	-0.1747 (0.0598)	0.0397 (0.0668)	0.0388 (0.0676)
σ	10.4233 (0.4991)	-	-	-	-	21.0979 (1.9572)	-	-	-	-
σ_0	-	1.1565 (0.0925)	1.1432 (0.1835)	2.3423 (0.0479)	1.1746 (3.0419)	-	1.8126 (0.1950)	1.2693 (0.4205)	3.0489 (0.0941)	2.5593 (5.4616)
σ_1	-	0.3112 (0.0187)	0.3173 (0.0751)	0.2389 (0.2239)	0.2462 (0.2243)	-	0.2372 (0.0307)	0.4342 (0.1344)	0.0058 (0.4084)	-0.4970 (5.5431)
σ_2	-	-	-0.0006 (0.0072)	-	-1.1825 (3.08)	-	-	-0.0157 (0.0103)	-	0.0133 (0.4157)
AIC	8712.62	8448.64	8450.63	8713.48	8715.33	1974.82	1915.96	1915.93	1976.82	1978.81
BIC	8722.80	8463.92	8471.00	8728.76	8735.70	1981.79	1932.42	1929.87	1987.28	1992.75
AICc	8712.63	8448.66	8450.66	8713.50	8715.36	1974.87	1916.16	1916.10	1976.92	1978.98
HQIC	8716.45	8454.39	8458.30	8719.23	8723.00	1977.63	1922.17	1921.55	1981.03	1984.43

Table 4 show the distribution parameters for the two selected regions and the evaluation criteria under stationary and non-stationary assumptions. Moreover, the lower AIC values conform to the presence of a stationary or non-stationary nature of the regions. The same procedure for threshold selection of the POT and the DPT discussed above can be implemented for all other regions. The thresholds obtained for region R2 from the POT are u=9.6 has n=1209, and DPT is u^*=30.5 has n=210; for region R3 from the POT is u=11 has n=1210, and DPT has u^*=30.48 and its n=248; for region R4 from POT is u=9.3 has n=1211, and DPT is u^*=27.08 has n=288; for region R5 from POT is u=8.4 has n=1203, and DPT is u^*=7.88 has n=1274; for region R6 from POT is u=9.5 has n=1205, and DPT is u^*=7.39 has n=1538; for region R7 from POT is u=11 has n=1189, and DPT is u^*=14.81 has n=820 obtained from the analysis. The stationary GP and non-stationary GP models that incorporate linear, quadratic, and cyclic covariates of wind speed and time in their scale parameter can be used for the analysis of the threshold exceedances from the two different POT and DPT methods for the chosen R1 as an illustration and all the remaining regions follow the same procedure. For NSGP1 and NSGP2, the wind speed is considered as the covariate, and for NSGP3 and NSGP4 the time is a covariate. For region R1, NSGP1 is the suitable model for the POT extremes and NSGP2 is the best one for DPT extremes these can be retrieved among the other four models using the measures of selection criteria. The most appropriate models selected for all seven regions are displayed in Table 5 for all three different methods of choosing extremes. The majority of regions in the POT series benefit significantly from the NSGP1 accounts for a linear variation of wind speed in the scale parameter, such as R1, R2, R5, and R6; R3 and R7 have NSGP2, which are quadratic variations of wind speed in the scale parameter; and R4 has NSGP3, which are cyclic or sinusoidal variations of time in the scale parameter of the GP as an appropriate model.

Table 5. The suitable models for selected regions

Region		Selected Models		
		AM-GEV	POT-GP	DPT-GP
Chennai	R1	GEV11	NSGP1	NSGP2
Chengalpattu	R2	GEV10	NSGP1	NSGP1
Thoothukudi	R3	GEV00	NSGP2	GP
Tirunelveli	R4	GEV00	NSGP3	NSGP3
Ramanathapuram	R5	GEV00	NSGP1	NSGP2
Virudhunagar	R6	GEV10	NSGP1	NSGP3
Kanyakumari	R7	GEV22	NSGP2	NSGP1

The extremes extracted from the DPT method can be modeled with stationary and non-stationary GP for all regions, via NSGP1 for region R2 and NSGP2 for regions R1, and R5 having wind speed as a covariate; NSGP3 for regions R4 and R6 having time as a covariate, and the stationary GP model for R3 respectively. Table 5 describes the suitable model for all seven

locations of extreme values that can be extracted from the AM, POT, and DPT methods. In this study, we observe that the non-stationary models to the series generally lead to a significant improvement in the model performance. The model performances also indicated that the inclusion of covariate (non-stationarity) provides a better model fit for the distributions.

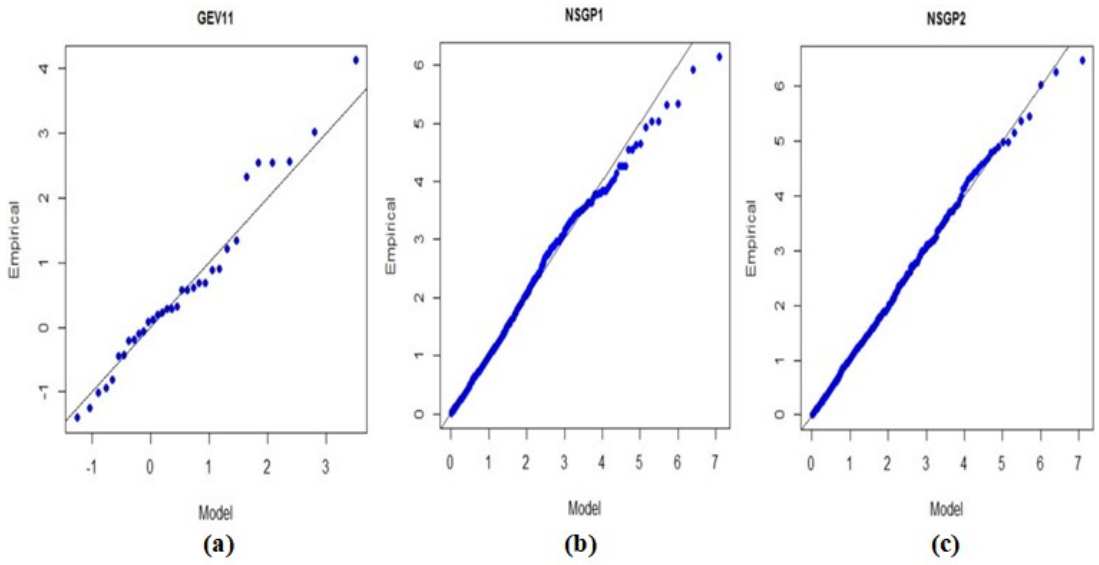

Fig 4. Q-Q plots for region R1

The quantile-quantile (Q-Q) plots of selected models from Table 5 of fitted and observed precipitation maxima are shown in Figure 4 which has been used to test the AM-GEV in **(a)** and POT-GP in **(b)** and DPT-GP in **(c)** model's goodness of fit for the region R1. The Q-Q plots in Figure 4 demonstrate how the stationary and non-stationary models differ significantly in their ability to fit the distribution's tail. The investigation of stationary and non-stationary models using the Q-Q plot aids in understanding model improvement. We utilized Q-Q plots to assess how well the best non-stationary models describe precipitation extremes in comparison to the stationary models. As a result, the non-stationary assumption with linear covariate model NSGP2 from the DPT technique is the optimum choice for region R1 and the same technique can be used for the remaining regions in their model selection. The results obtained by comparison of the non-stationary or stationary model at each region for the daily precipitation are shown in Table 6. It was observed that the POT method of extremes with non-stationary GP is a suitable model for two regions R3 and R5; the DPT method of extremes with non-stationary GP is a suitable model for all other five regions. This study concluded that the non-stationary models are more suitable for the POT and DPT approaches than the stationary state, indicating that it is appropriate for the precipitation series. The extreme precipitation values of return levels at different return periods such as 2, 5, and 10 years are estimated for the selected regions during stationary and non-stationary conditions in the models. Various return periods for the same region have been shown in Figure 5. The performance of the non-stationary GP model over the observed POT and DPT excesses was evaluated for the precipitation levels of various return periods. Consider using models that allow for changes in GP parameters over time or incorporate wind speed as covariates to capture temporal variations.

Table 6. The Suitable model for regions R1 to R7

Region	Model	scale	shape (ξ)	AIC	BIC	AICc
R1	DPT-NSGP2	σ_0= 1.2693 (0.4205) σ_1= 0.4342 (0.1344) σ_2= -0.0157 (0.0103)	-0.1642 (0.0575)	1915.93	1929.87	1916.10
R2	DPT-NSGP1	σ_0=1.9350 (0.2309) σ_1=0.1934 (0.0328)	-0.1658 (0.0549)	1661.66	1671.7	1661.78
R3	POT-NSGP2	σ_0= 1.7038 (0.2082) σ_1= 0.1914 (0.0966) σ_2= -0.0133 (0.0104)	0.1861 (0.0339)	8222.92	8243.28	8222.95

Continued on next page

Table 6 continued

R4	DPT-NSGP3	σ_0= 2.6821(0.091) σ_1=1.1327(0.438)	0.1392(0.060)	2256.07	2270.72	2256.21
R5	POT-NSGP1	σ_0= 1.9454(0.092) σ_1=0.0534(0.019)	0.1336(0.033)	7975.11	7990.38	7975.12
R6	DPT-NSGP3	σ_0=2.160(0.0391) σ_1=0.8316(0.176)	0.1349(0.0294)	10217.73	10233.74	10217.74
R7	DPT-NSGP1	σ_0= 2.3057(0.122) σ_1= 0.0519(0.018)	0.1592 (0.041)	6188	6202.12	6188.02

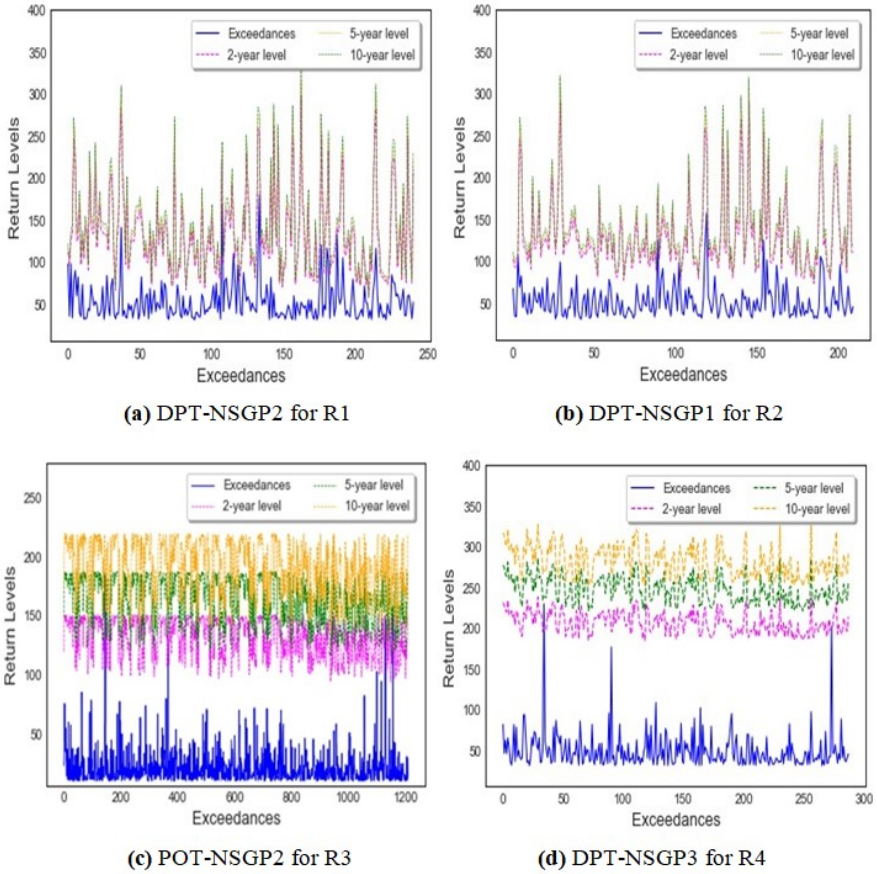

(a) DPT-NSGP2 for R1 **(b)** DPT-NSGP1 for R2

(c) POT-NSGP2 for R3 **(d)** DPT-NSGP3 for R4

Fig 5. The 2, 5, and 10-year return levels of precipitation using the suitable model for all regions

In Figure 5, the blue line represents the series of exceedances above the chosen threshold, and the corresponding estimated maximum precipitation level for 2, 5, and 10 return periods is shown for R1 to R4 regions as an illustration. In Figure 5, the return period lines assist in visualizing the probability of an occurrence exceeding a specific threshold in a given year. The x-axis typically represents the threshold exceedance level. This is the level above which extreme events are considered. The y-axis represents the return level, which is the expected value of the exceedance level depending on the wind speed or time that it has been exceeded. It is essentially the quantile function of the GP distribution. The different models and parameterizations may yield distinct patterns in the return level lines. Sudden changes in slope or pattern may indicate shifts in the underlying process. In this study, we observe that when there is an increase in the return period there must be an increase in the return level estimates as shown in Figure 5. We should consider the changing return levels for the practical implications. Here, the return-level estimates of extreme events in non-stationary conditions are made based on the end of the data period, the year 2023. For instance, in the context of flooding, increasing precipitation return levels may have implications for infrastructure planning and risk management. Overall, accounting for the non-stationary conditions considering the natural or anthropogenic activities, the non-stationary frequency analysis is better for estimating the meteorological variables in different design periods.

4 Conclusion

In this study, the effect of nonstationarity was investigated by comparing the performance of stationary and non-stationary GEV and GP models that can be used to describe data variability in exceedances from classical and proposed DPT methods of threshold selection. The main focus is on nonstationarity in the location and scale parameters of distributions expressed as linear and nonlinear functions of wind speed and time resulting in a significant improvement in modeling precipitation extremes when compared to their stationary counterparts. This study highlights that the estimation of precipitation changes markedly depending on the approach to extracting extreme events as demonstrated graphically by the 2, 5, and 10-year return level estimates for seven regions. A tendency was found that the precipitation estimated by DPT extremes modeled with non-stationary GP was preferably better at most of the stations than POT with non-stationary GP models. It should be identified that the estimates of precipitation from non-stationary models provide a better representation of the distribution tail than the estimates from stationary models when planning the design and operation of water facilities. Furthermore, the planning process under stationary assumptions becomes more sensitive to catastrophes like floods which are predicted to occur by climate models, as well as an increase in the frequency of heavy rain occurrences. Non-stationarity was represented in the GEV and GP models by parameters stated as linear and nonlinear covariate functions, respectively. Furthermore, a basic assumption underpins the current study: the impact of changing climate propagates into changes in extreme characteristics of covariates; that is, wind speed and time are examined to account for non-stationarity in precipitation extremes. This case study exemplifies the need to employ non-stationary models to account for possible dependencies between the variable of interest and other factors to improve estimation quality. As an illustration, such a tool might be extremely helpful in constructing environmental preventive models that account for climatic variations.

References

1) Ouarda TBMJ, Charron C. Changes in the distribution of hydro-climatic extremes in a non-stationary framework. *Scientific Reports*. 2019;9(1):1–8. Available from: https://dx.doi.org/10.1038/s41598-019-44603-7.
2) Kumar D, Gautam YP, Kumar V, Kumar S, Saradhi IV, Kumar AV. Statistical analysis of extreme value of meteorological elements observed for the last 31 years (1989-2019) at the Narora site. *Radiation Protection and Environment*. 2021;44(3&4):123–123. Available from: https://dx.doi.org/10.4103/rpe.rpe_27_21.
3) Baldan D, Coraci E, Crosato F, Ferla M, Bonometto A, Morucci S. Importance of non-stationary analysis for assessing extreme sea levels under sea level rise. *Natural Hazards and Earth System Sciences*. 2022;22(11):3663–3677. Available from: https://dx.doi.org/10.5194/nhess-22-3663-2022.
4) Rohmer J, Thieblemont R, Cozannet GL. Revisiting the link between extreme sea levels and climate variability using a spline-based non-stationary extreme value analysis. *Weather and Climate Extremes*. 2021;33:1–12. Available from: https://dx.doi.org/10.1016/j.wace.2021.100352.
5) Prahadchai T, Shin Y, Busababodhin P, Park JS. Analysis of maximum precipitation in Thailand using non-stationary extreme value models. *Atmospheric Science Letters*. 2023;24(4):1–11. Available from: https://dx.doi.org/10.1002/asl.1145.
6) Kim H, Kim T, Shin JY, Heo JH. Improvement of Extreme Value Modeling for Extreme Rainfall Using Large-Scale Climate Modes and Considering Model Uncertainty. *Water*. 2022;14(3):1–22. Available from: https://dx.doi.org/10.3390/w14030478.
7) Wang Y, Peng T, Lin Q, Singh VP, Dong X, Chen C, et al. A New Non-stationary Hydrological Drought Index Encompassing Climate Indices and Modified Reservoir Index as Covariates. *Water Resources Management*. 2022;36(7):2433–2454. Available from: https://dx.doi.org/10.1007/s11269-022-03151-y.
8) Kumar N, Patel P, Singh S, Goyal MK. Understanding non-stationarity of hydroclimatic extremes and resilience in Peninsular catchments, India. *Scientific Reports*. 2023;13(1):1–13. Available from: https://dx.doi.org/10.1038/s41598-023-38771-w.
9) Khan MU, Ijaz MW, Iqbal M, Aziz R, Masood M, Tariq MAUR. Impact Evaluation Using Nonstationary Parameters for Historical and Projected Extreme Precipitation. *Water*. 2023;15(22):1–18. Available from: https://dx.doi.org/10.3390/w15223958.
10) Wu G, Qiu W. Threshold Selection for POT Framework in the Extreme Vehicle Loads Analysis Based on Multiple Criteria. *Shock and Vibration*. 2018;2018:1–9. Available from: https://dx.doi.org/10.1155/2018/4654659.
11) Galib AH, Mcdonald A, Wilson T, Luo L, Tan PN. DeepExtrema: A Deep Learning Approach for Forecasting Block Maxima in Time Series Data. In: Proceedings of the Thirty-First International Joint Conference on Artificial Intelligence. International Joint Conferences on Artificial Intelligence Organization. 2022;p. 2980–2986. Available from: https://www.ijcai.org/proceedings/2022/0413.pdf.
12) Pahrany AD, Aeli LW, Mukhaiyar U. Value at risk analysis using automated threshold selection method in property insurance. In: The 3rd International Conference on Mathematics and its Applications (ICOMATHAPP) 2022: The Latest Trends and Opportunities of Research on Mathematics and Mathematics Education;vol. 3049, Issue 1 of AIP Conference Proceedings. AIP Publishing. 2024. Available from: https://doi.org/10.1063/5.0193668.
13) Coles S. An Introduction to Statistical Modeling of Extreme Values;vol. 208 of Springer Series in Statistics. 1st ed. London. Springer. 2001. Available from: https://doi.org/10.1007/978-1-4471-3675-0.
14) Scarrott C, MacDonald A. A review of extreme value threshold estimation and uncertainty quantification. *REVSTAT - Statistical journal*. 2012;10(1):33–60. Available from: https://www.ine.pt/revstat/pdf/rs120102.pdf.
15) Trung DD. A combination method for multi-criteria decision making problem in turning process. *Manufacturing Review*. 2021;8:1–17. Available from: https://dx.doi.org/10.1051/mfreview/2021024.
16) Zhu Y, Tian D, Yan F. Effectiveness of Entropy Weight Method in Decision-Making. *Mathematical Problems in Engineering*. 2020;2020:1–5. Available from: https://dx.doi.org/10.1155/2020/3564835.